We are IntechOpen, the world's leading publisher of Open Access books Built by scientists, for scientists

4,800
Open access books available

122,000
International authors and editors

135M
Downloads

Our authors are among the

154
Countries delivered to

TOP 1%
most cited scientists

12.2%
Contributors from top 500 universities

CLARIVATE ANALYTICS BOOK CITATION INDEX INDEXED

WEB OF SCIENCE™

Selection of our books indexed in the Book Citation Index in Web of Science™ Core Collection (BKCI)

Interested in publishing with us?
Contact book.department@intechopen.com

Numbers displayed above are based on latest data collected.
For more information visit www.intechopen.com

17

Micro Swimming Robots Based on Small Aquatic Creatures

Seiichi Sudo
Akita Prefectural University
Japan

1. Introduction

Earth is a sphere of life. All living things are capable of movement. Animals occur almost everywhere and make up more than half of all the living things on this planet. Most animals move about using legs, wings, or fins. The swimming of a variety of aquatic living creatures and the flying of insects have been a source of continuous fascination to scientists working in many fields. The importance of the locomotive functions of animals is well recognized with respect to a variety of robot developments. Extensive investigations on the biokinetics of swimming and flying animals have been conducted and reported by a number of researchers (Alexander, 1984; Azuma, 1992; Dickinson et al., 2000). Body size and shape of living creatures are a natural result of the adaptation of the manner of movement to environmental conditions (Azuma, 1992). In general, swimming is a far more economical way to move to a distant point than flying. Almost all swimming creatures are considerably longer in the swimming direction. The swimming motions of small aquatic creatures are fascinating to behold. With increasing interest hydrodynamicists have studied the interactions of these creatures with their surrounding fluid medium (Blake, 1972; Dresdner et al., 1980; Daniel, 1984; Jiang et al., 2002a; 2002b; 2002c). In spite of many investigations, however, there still remains a wide unexplored domain. Especially, in order to develop minute micro robots and micro mechanisms, the swimming analyses of smaller living creatures are demanded (Sudo et al., 2009). In this chapter, the swimming behaviour of small aquatic creatures was analyzed by a digital high-speed video camera system. Various swimming modes of small aquatic creatures were clarified experimentally. Furthermore, based on the swimming analyses of small aquatic creatures, some wireless micro swimming robots were made for trial purposes. Those micro swimming robots composed of a permanent magnet were driven by the external alternating magnetic field. The swimming characteristics of those micro robots were also examined, and frequency characteristics for swimming velocity of micro robots were revealed.

2. Experimental Apparatus and Procedure

Experiments on small aquatic creature swimming are conducted with a high-speed video camera system shown in authors' previous paper (Sudo et al., 2008). A schematic diagram of

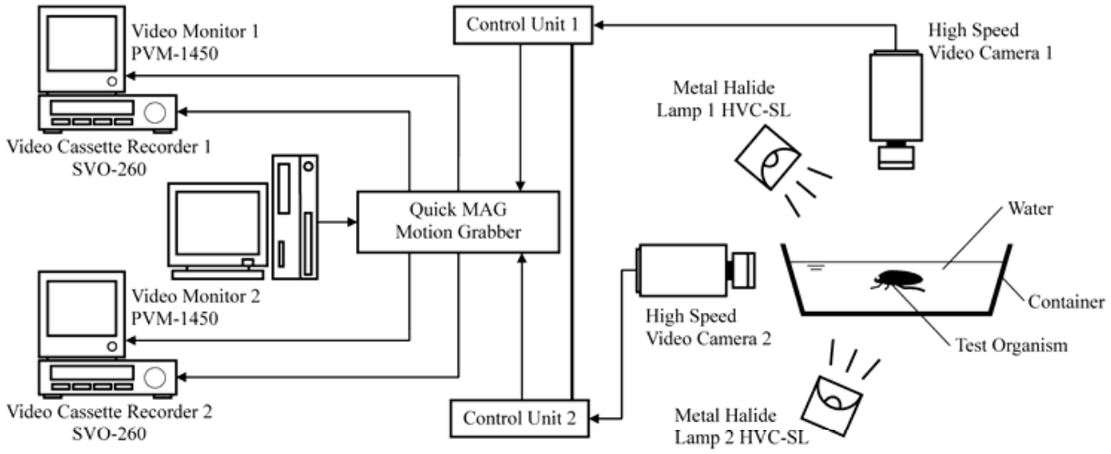

Fig. 1. Schematic diagram of experimental apparatus for free swimming analysis of small aquatic creatures

the experimental apparatus is shown in Fig.1. Some kinds of rectangular and cylindrical containers with different sizes were used in the experiments. The experimental apparatus consists of the swimming water container system, the measurement system, and the analysis system. The containers were produced with transparent acrylic plastic for optical observation. The sizes of the containers were changed by test aquatic creatures. The containers were filled up to the certain depth with water or seawater according to the test aquatic creatures. The small aquatic creatures were released in the water container. Free swimming of the test aquatic creature was observed optically with the high-speed video camera. A series of frames of free swimming behaviour of test aquatic creature were analyzed by the personal computer. In the experiment of tethered swimming analyses, the test live aquatic creature was pasted up on a human hair or a thin needle with the adhesive. The motions of the swimming legs of test aquatic creature were recorded by the high-speed video camera. A series of frames of the leg motions during swimming behaviour were also analyzed by the personal computer. In the experiment for flow visualization, the powder of chaff was scattered in the water. Movement of powder was photographed with 35mm camera. The experiments were conducted under the room temperature in summer (water temperature 18-22℃). For the purpose of the investigation on the morphological structure of swimming legs of small aquatic creatures, microscopic observations were conducted with a scanning electron microscope.

3. Swimming of Diving Beetles

3.1 Family Dytiscidae

Family Dytiscidae is one of large aquatic families with 177 species in 37 genera(Zborowski & Storey, 1995). They are found in streams, shallow lakes and ponds, brackish pools, and themal springs. They range from 1 to 40 mm in length, and are very smooth and mostly oval for rapid underwater movement. Most species are black or dark brown but some have yellow, blown, or green marking. The hind legs are enlarged and the tarsi have a border of

Fig. 2. Dorsal view of diving beetle, Cybister japonicas Sharp

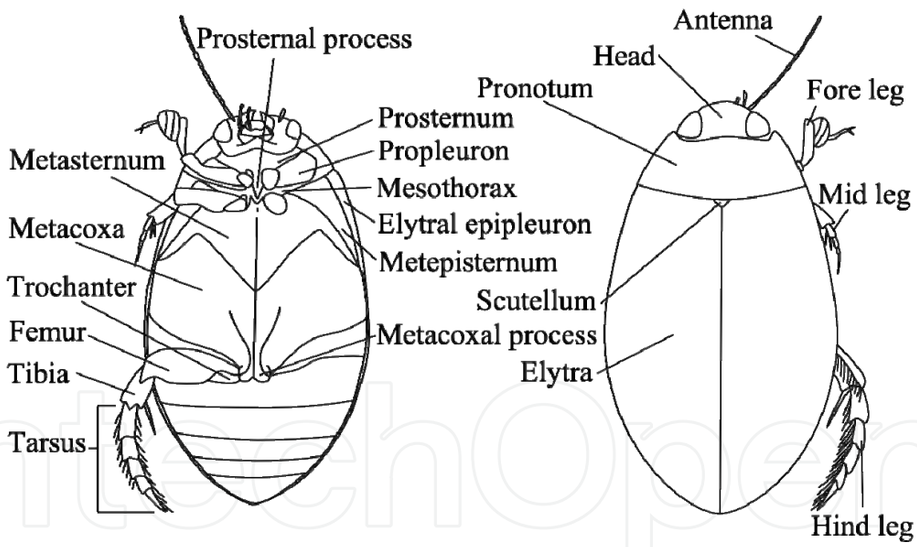

Fig. 3. A typical adult diving beetle illustrating the major parts of the body

hairs acting as oars when the legs beat in unison. The hind coxae extend to the elytra on the sides and the antennae are filiform. Highly adapted for aquatic life, they breathe by comming to the surface backwards and exposing the tip of the abdomen which draws in air to store under the elytra. They are fierce predators, attacking various preys, from insects to frogs and small fish. In this experiment, test insects were collected in stream and ponds. A diving beetle, *Cybister japonicus* Sharp, captured at Yurihonjo in Japan is shown in Fig.2. The rowing hind legs with hairs are clear in Fig.2. Figure 3 shows a schematic diagram of an

adult diving beetle and the named body parts. Adult insects have a general body plan of three main divisions; head, thorax and abdomen. In the experiment, test diving beetles were *Gaurodytes japonicas*, *Cybister lewisianus*, *Cybister japonicus*, and *Hydrogyphus japonicus*.

3.2 Swimming Behavior of diving beetle

As was stated previously, shape of diving beetles is often distinctive; elongate-oval, convex, streamlined. The hind legs are flattened and fringed with hairs. The hind tarsi have 1 or 2 claws. They are excellent swimmers, and usually when swimming move the hind legs in unison. Dytiscid beetles are the most extensively studied of these insect rowers, with excellent measurements of limb and body kinematics and drag coefficients (Nachtigall, 1980). However, the research data on the swimming behaviour of diving beetles are insufficient, and there still remains a wide unexplored domain. In this paragraph, the swimming behaviour of diving beetle in water container was examined. Figure 4 shows a sequence of photographs showing the free swimming behaviour of diving beetle. It can be seen that the

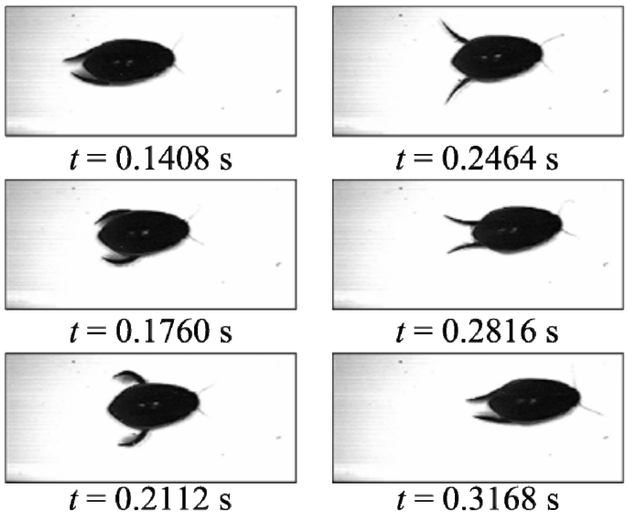

Fig. 4. A sequence of photographs showing the swimming behaviour of the diving beetle

diving beetle swims by flexing his hind legs together. During the power stroke, they are stretched and move backward. The thrust-generating mechanism is related to the motion of the hind legs. Four characteristic points on the diving beetle body were defined by the signs shown in Fig.5. These points correspond to head (H0), tail (T0), and right and left hind legtips (R3 and L3 respectively). Figure 6 shows the legtip, head, and tail orbits and the body orbit during swimming of the diving beetle. In Fig.6, L is the body length of the diving beetle, and δ_t is the time interval of plotting data. Arrows indicate the direction of the movement of the diving beetle. The orbits of right and left legtips show almost the same. The diving beetle swims by paddling its flexible hindlegs. The articulated hindlegs with hairs are fully extended in power stroke, but folded and narrowed in the recovery stroke. Let us consider the thrust-generating mechanism in a diving beetle moved with a constant velocity U. To simplify the following calculations, the leg is assumed to move backward along a straight line with a constant velocity V_p. The driving force T_p generated by the fluid

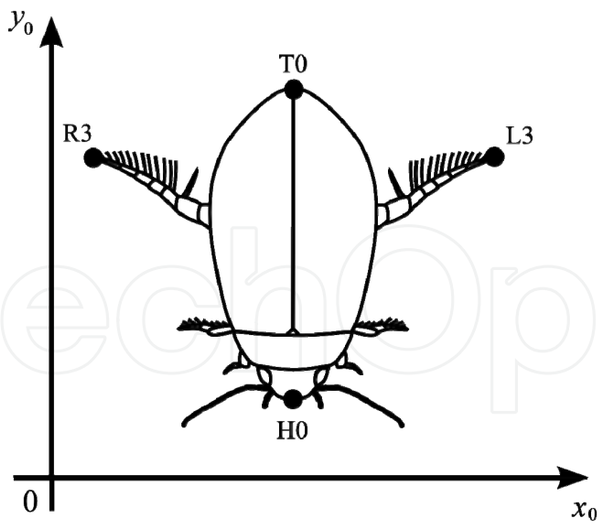

Fig. 5. Definition of signs of measurement points on the diving beetle

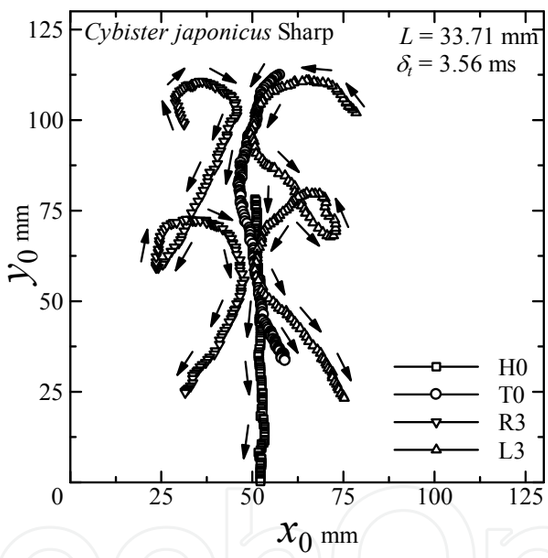

Fig. 6. Swimming trajectories of hind legtips, head, and tail of the diving beetle

dynamic drag of the leg, which is proportional to the dynamic pressure of the relative speed V_p-U, can be expressed as follows (Azuma, 1992);

$$T_p = \frac{1}{2}\rho\left(V_p - U\right)\left|V_p - U\right|S_p C_D \tag{1}$$

where S_p is the frontal area, and C_D is the drag coefficient. Here the inertia force has been neglected. The power P required to drive the drag is given by Eq. (2).

$$P = T_p V_p = \frac{1}{2}\rho V_p \left(V_p - U\right)\left|V_p - U\right| S_p C_D \tag{2}$$

In the power stroke at constant water beetle speed U, the body drag of the diving beetle D, and necessary power of the diving beetle W, are given as follows;

$$D = \frac{1}{2}\rho U^2 S_T = T_p \tag{3}$$

$$W = DU = T_p U = \frac{1}{2}\rho U^3 S_T \tag{4}$$

where S_T is the drag area of the diving beetle body. In the recovery stroke, the negative driving force T_r can be neglected, because the hindlegs are folded and swimming hairs are laid against the leg. Thus, hydrodynamic efficiency can be given as follows;

$$\eta = \frac{W}{P} = \frac{U}{V_p} = \frac{1}{1 + \sqrt{\dfrac{S_T}{S_p C_D}}} \tag{5}$$

It can be seen from Eq. (5) that $S_T/S_pC_D \to 0$ means higher hydrodynamic efficiency in swimming of diving beetles. In an actual diving beetle, the drag coefficient of a leg C_D is unsteady and strongly dependent on the leg structure. The diving beetle is a small insect characterized by short forelegs and long hindlegs with hairs to provide propulsion. The mean drag coefficient of a rectangular flat plate in normal flow is a function of the aspect ratio of the plate and the Reynolds number (Azuma, 1992). It changes from C_D=1.2 to C_D=2.0. The mean drag coefficient of a column is also a function of the Reynolds number Re as follows;

$$C_D = \frac{10.9}{Re\left(0.87 - \log Re\right)} \tag{6}$$

This equation states that the drag coefficient increases decreasing in the Reynolds number. If the flat plate leg is replaced with the set of a lot of minute columns, the drag also increases. The hind legs composed of a lot of minute hairs may generate higher drag. Since a rowing hair of diving beetle is from 20 to 2 μ m in diameter from base to tip (Nachtigall, 1980a), the flow around hairs of the leg is a lower Reynolds number flow. The value of S_T/S_pC_D in Eq.(5) becomes smaller with an increase in C_D. In an actual swimming of diving beetle, the driving force T is described by the difference between T_p in the power stroke and T_r in the recovery stroke, because the legs oscillate back and forth.

$$T = T_p - T_r \tag{7}$$

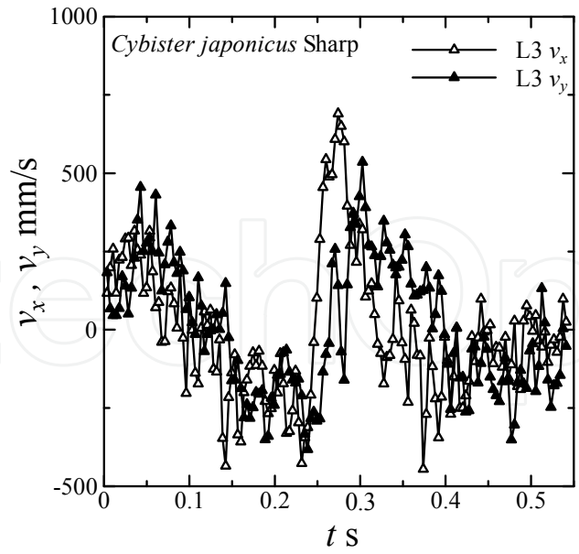

(a) Velocity components of legtip motion

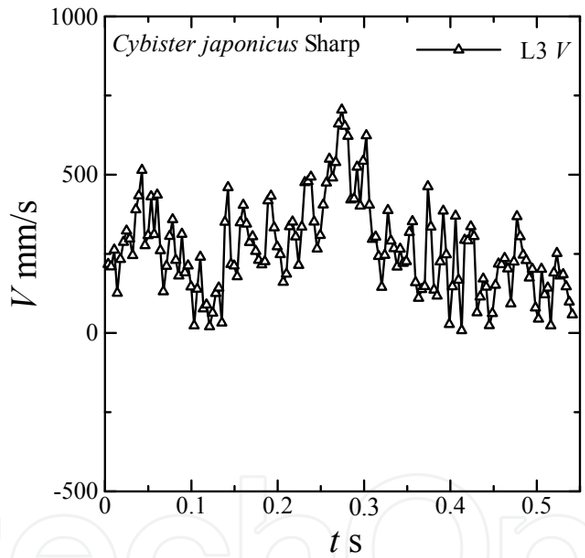

(b) Two dimensional velocity of legtip motion

Fig. 7. Velocity variations of legtip motion during swimming of the diving beetle

Therefore, the swimming motion of diving beetle is unsteady. Fig.7 shows the velocity variations in the legtip motion of the diving beetle during swimming. The speed change in hind leg corresponds to propulsion of the entire body with diving beetle swimming. In Fig.7, v_x and v_y are x and y components of the legtip velocity respectively, and V is the two dimensional velocity described by $V=(v_x^2+v_y^2)^{1/2}$. Diving beetles swim with their strong hindlegs that they use like oars on a rowboat. If the shape of the hindlegs does not change, a quasi-steady analysis finds that the net force for a cycle of oscillation is zero. Fig.7 shows a periodic change of the velocity of the left hindlegtip. The time range of a rapid increase in

the velocity corresponds to the power stroke. On the other hand, a slowly decrease of the velocity corresponds to the recovery stroke. The diving beetle enlarges the driving force T_p, and reduces T_r.

3.3 Swimming Behavior of Small Diving Beetle

There is an interesting diving beetle that shows different swimming from usual diving beetles. In general, the third pair of legs (hindlegs) in usual diving beetles beat synchronously during the power stroke. In this paragraph, the swimming behaviour of a diving beetle, *Hydroglyphus japonicas* Sharp, is shown. The diving beetle, *Hydroglyphus japonicas* Sharp, is a small insect with the body length about 2mm as shown in the photograph in Fig.8. This test insect was collected in the rice field at Yuri Honjo in Japan . The diving beetle is confined in the water drop in Fig.8. Figure 9 shows a sequence of photographs of swimming behaviour of the diving beetle, *Hydroglyphus japonicas* Sharp. It can be seen that the diving beetle swims by alternately rowing his hind legs. In other words, the diving beetle swims by alternately paddling of right and left hind legs. Small channel with 3.3 mm in width and 3 mm in depth was used in this experiment. This channel is composed of the ditch on the tree plate and tap water. Figure 10 shows the legtip, head, and tail orbits and the body orbit during swimming of the diving beetle. The head orbit of the insect draw the sinusoidal curve, that is, the head swings right and left according to rowing the hind legs. It is uncertain why the diving beetle, *Hydroglyphus japonicas* Sharp, swims in a zigzag line. When the small diving beetle swims in mud, such swimming mode must be convenient. Fig.11 shows the velocity variations in the left hind legtip motion of the diving beetle during swimming. The variation of the velocity component of legtip motion in two dimension cordinate system is shown in Fig.11(a), and the variation of two dimensional

Fig. 8. Photograph of a small diving beetle, *Hydroglyphus japonicas* Sharp, in a water drop

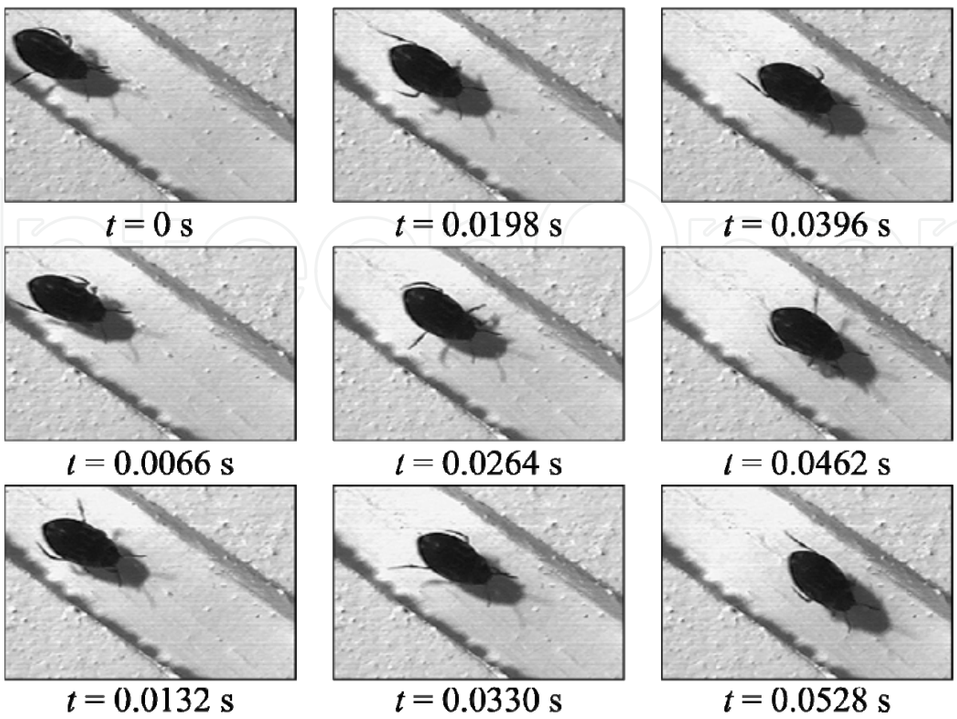

Fig. 9. A sequence of swimming behaviour of the small diving beetle in a narrow waterway

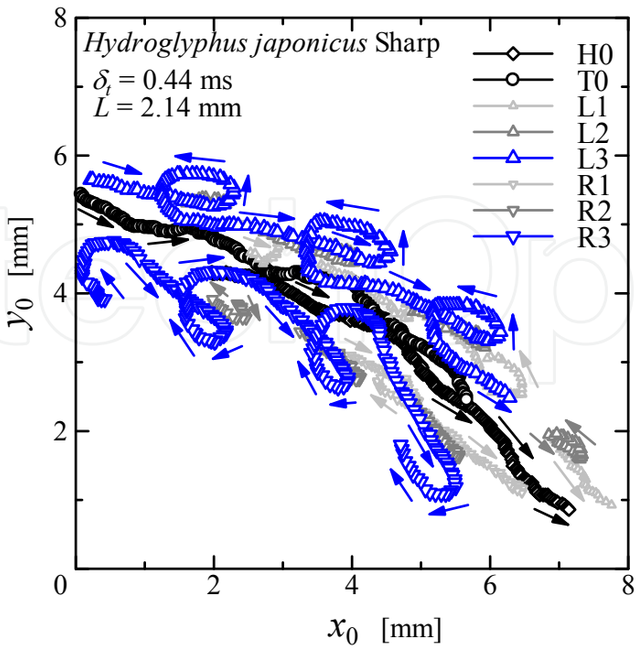

Fig. 10. Swimming trajectories of legtips, head, and tail of the diving beetle

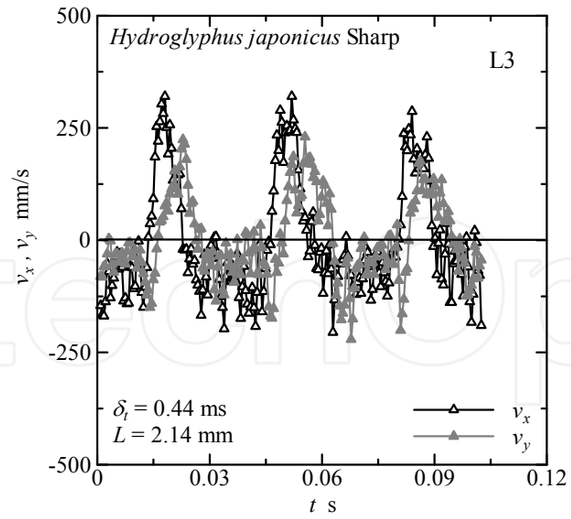

(a) Velocity components of legtip motion

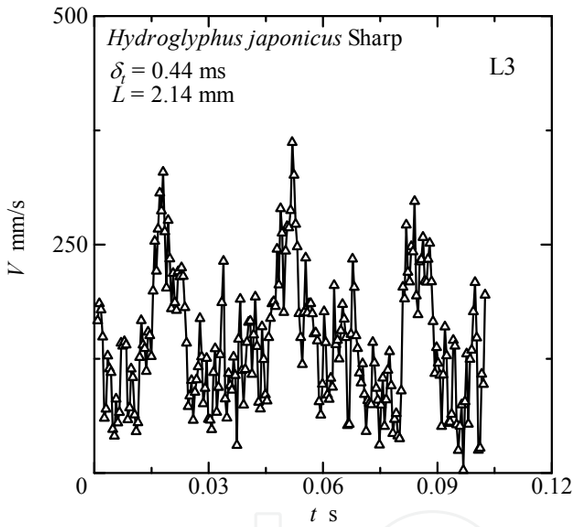

(b) Two dimensional velocity of legtip motion

Fig. 11. Velocity variations of legtip motion during swimming of the diving beetle

Fig. 12. Electron micrograph of a part of swimming leg of the diving beetle

resultant velocity is shown in Fig.11(b). Sharp rising up of the velocity variation corresponds to the power stroke, and gradual decreasing corresponds to the recovery stroke during swimming of the diving beetle. As stated above, swimming legs of the diving beetle, *Hydroglyphus japonicas* Sharp, are also clothed in minute hairs. The hairs increase the hydrodynamic drag of the swimming leg. Scanning electron microscopic observation of the swimming legs of the diving beetle shows existence of fine hairs on the legs. Figure 12 shows scanning electron micrograph of the rowing appendages and fine hairs of the diving beetle, *Hydroglyphus japonicas* Sharp. The thickness of the hair is about 1.5 μ m in Fig.12.

4. Swimming of Dragonfly Nymph

After the dragonfly nymph emerges from the egg, it develops through a series of stages called instars. The dragonfly larvae are predatory and live in all types of freshwater. The younger nymph was selected as a test insect in the swimming experiment, because the younger nymph swam actively. The tested nymph shown in Fig. 13 was a larva of dragonfly, *Sympetrum frequens*. The swimming behavior of the nymph in water container was examined. Fig.14 shows a sequence of photographs showing the swimming behavior of dragonfly

Fig. 13.Photograph of a younger small dragonfly nymph used in the swimming experiment

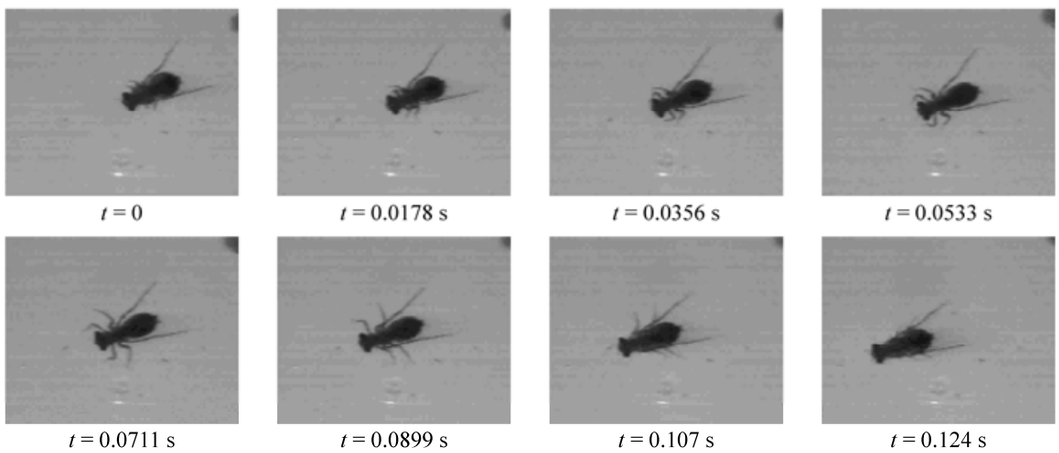

Fig. 14. A sequence of photographs showing the swimming behavior of the dragonfly nymph in water container

nymph. The process of leg movement for the nymph swimming is clear. The fore- and middle-legs beat almost synchronously. During the power stroke they are stretched and move. On the other hand, the hind-legs hardly move. The thrust-generating mechanism is related to the motion of the fore- and middle-legs. The dragonfly nymph expands and contracts its abdomen to move water during forward swimming. Figure 15 shows the change in the size of the nymph body through the swimming stroke. The changes of the body length L_s and the body width W_s are the opposite phases. The body length L_s and the body width W_s through the straight swimming are described as follows;

$$\left.\begin{aligned} L_s &= L + \alpha \sin(\omega t + \phi) \\ W_s &= W + \beta \sin(\omega t - \pi + \phi) \end{aligned}\right\} \tag{8}$$

where ω is the angular frequency of swimming stroke, t is the time, ϕ is the phase difference with the leg motion, and α and β are constants. In this experiment, constants α and β are described as follows;

$$\left.\begin{aligned} \alpha &= 0.60\,\text{mm} \\ \beta &= 0.25\,\text{mm} \end{aligned}\right\} \tag{9}$$

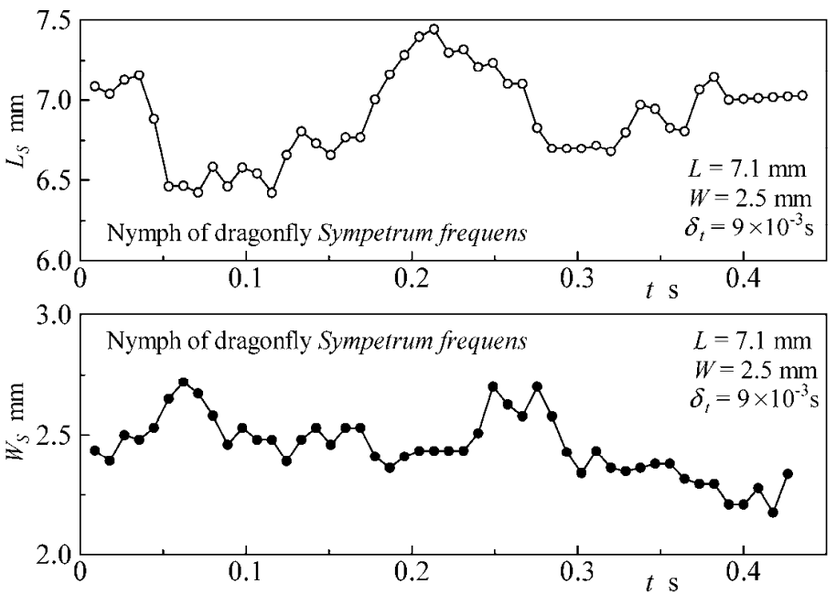

Fig. 15. Expansion and contraction of the nymph body during swimming

The change in the body size of tested nymph was about 10%. The legtips move at higher seed during the power stroke, and lower speed during the recovery stroke. Such a leg

movement generates the thrust force for nymph swimming. The swimming number S_w of this tested nymph is the following value;

$$S_w = \frac{V_{mean}}{f_s L} = \frac{77.6}{5.0 \times 7.1} \approx 2.2 \tag{10}$$

where V_{mean} is the mean swimming velocity, and f_s is the paddling frequency. The swimming number shows how many body length per beat to swim. The swimming number S_w = 2.2 is larger compared with fish.

5. Micro Swimming Mechanism

5.1 Driving Principle of Micro Swimming Mechanism

The biomimetic study on the swimming robot was performed. As mentioned above, small aquatic creatures swim by using their swimming legs as underwater paddles to produce hydrodynamic drag. Based on the above-mentioned swimming analysis of the aquatic creatures, the micro swimming mechanism was produced by trial and error. The micro swimming mechanism is composed of polystyrene foam body, permanent magnet, polyethyleneterephthalate film fin, copper fin stopper, and tin balancer. The dimensions of the swimming mechanism are shown in Fig.16. The swimming mechanism is propelled by the magnetic torque acting on the small permanent magnet in the alternating magnetic field. The magnet is made of NdFeB alloy, and shape is a cube of 5mm×5mm×5mm. Table 1 shows the physical properties of NdFeB permanent magnet used in the experiment. Table 2 shows the magnetic properties of the permanent magnet. The experimental apparatus is almost similar to Fig.1, but the cylindrical container coiled electric wire was used to drive the swimming robot. When the alternating magnetic field is applied to the permanent magnet, the magnet oscillates angularly due to magnetic torque and drives the propulsive robot in water. The alternating magnetic field was generated by applying AC voltage to the coil wound around container. The alternating current signal was supplied from a frequency synthesizer. A block diagram of the coiled water container and measuring devices is shown in Fig.17. The magnetic torque $\boldsymbol{T_m}$ acting on the permanent magnet with magnetic moment $\boldsymbol{m}$ in the external magnetic field $\boldsymbol{H}$ is described by Eq.(11);

$$\boldsymbol{T_m} = \boldsymbol{m} \times \boldsymbol{H} \tag{11}$$

In this experiment, the external magnetic field was produced by the coil applied AC voltage;

$$E_c = \frac{E}{2} \sin\left(2\pi f_0 t\right) \tag{12}$$

where E is the total amplitude of AC voltage, f_0 is the frequency of AC voltage, and t is the time. Therefore, the external magnetic field generated by the coil is given by Eq.(13);

$$\boldsymbol{H} = H_0 \boldsymbol{e} \sin\left(2\pi f_0 t\right) \tag{13}$$

where H_0 is the amplitude of alternating magnetic field, $\boldsymbol{e}$ is a unit vector. Oscillating torque motion of the permanent magnet is excited by Eq.(13). The direction of the external magnetic

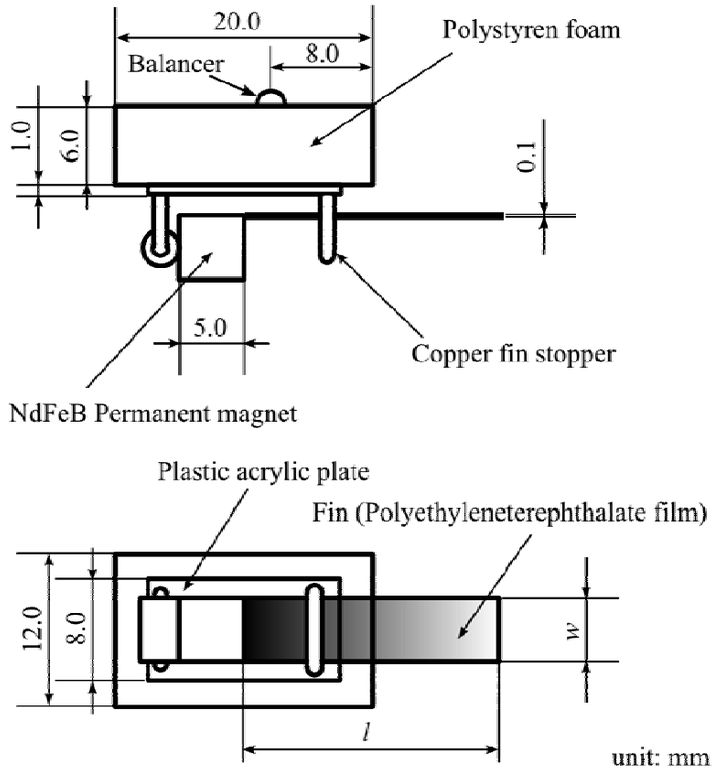

Fig. 16. Shape and dimension of the micro swimming mechanism

Permanent magnet	$Nd_2Fe_{14}B$
Temperature coefficient	0.12 % / ºC
Density	7300 - 7500 kg/m^3
Curie temperature	310 ºC
Vickers hardness	HV 500 - 600

Table 1. Physical properties of permanent magnet used in the experiment

Residual magnetic flux density *Br*	1.62 - 1.33 T
Coercive force *bHC*	859 - 970 kA/m
Coercive force *iHC*	> 955 kA/m
Maximum energy product $(BH)_{max}$	302 - 334 kJ/m^3

Table 2. Magnetic properties of NdFeB magnet used in the experiment

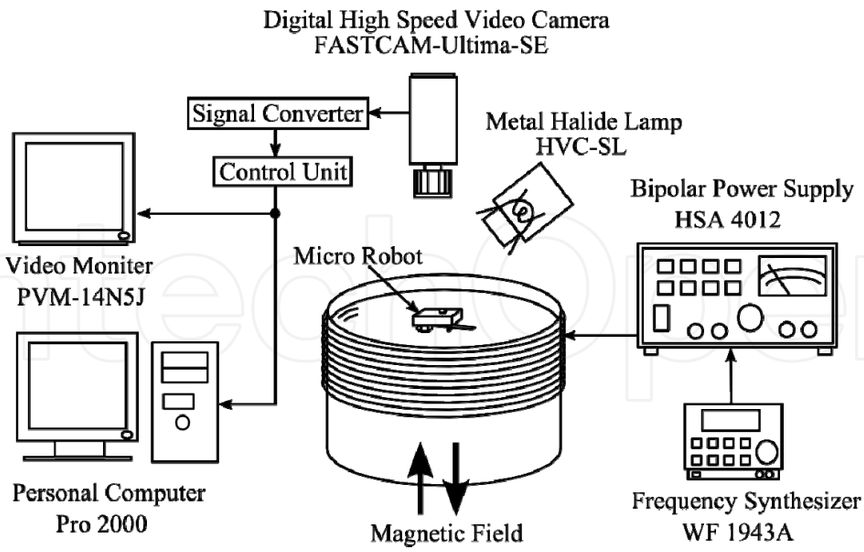

Fig. 17. Schematic diagram of experimental apparatus for locomotive characteristics of swimming robot

field is a vertical direction against the water level as shown in Fig.17. The magnet movement is connected with the fin motion directly. This mechanism swims by hydrodynamic drag produced by sweeping the fin. During one cycle of the swimming movement, the fin presses backwards against the water and this pushes the body forwards.

5.2 Frequency Characteristics of Swimming Velocity

The swimming behavior of the micro mechanism was observed with the experimental apparatus shown in Fig.17, that is, the swimming velocity of micro mechanism was examined within a certain frequency range of alternating magnetic field. In this experiment, the external magnetic field was generated with the coil around the water container shown in Fig.17. The experiment was performed on the condition of constant E in Eq.(12). Figure 18 shows the frequency characteristics of swimming velocity for the micro mechanism. In Fig.18, v is the swimming velocity, l is the fin length, w is the fin width, and the dotted lines show the unstable swimming of the micro mechanism. The effect of the applied voltage E is also shown in Fig.18. In general, an increase in the applied voltage E improves the swimming velocity of the micro mechanism. The increase in the applied voltage corresponds to the increase in the magnetic field generated by the coil. It can be seen from Fig.18 that the swimming velocity v depends on the frequency of alternating magnetic field f_0. The spectrum of the swimming velocity in Fig.18 has the peak at the range of f_0=4-6Hz. The peak frequency is related to the oscillation mode of the fin in water. The swimming velocity of the micro mechanism depends on the amplitude of fin oscillation. The larger amplitude leads to higher velocity of micro mechanism swimming. The micro mechanism swims by the fin oscillation. The flow field produced by the fin oscillation was examined. The flow field around the micro mechanism was visualized by slow shutter speed photograph. Figure 19 shows one example of flow visualization on the water surface around the micro mechanism. Flow visualization was created by floating powder on the water

surface. The shutter speed of the camera is 1/2 seconds. The swimming advancement of the micro mechanism is stopped with the wire of aluminum. The forward and backward flows are generated, but the backward flow is strongly generated. The speed difference between forward and backward flows is the swimming speed of the mechanism. Figuer 20 shows the flowfield produced by the live tethered opposum shrimp for the comparison. A stream is

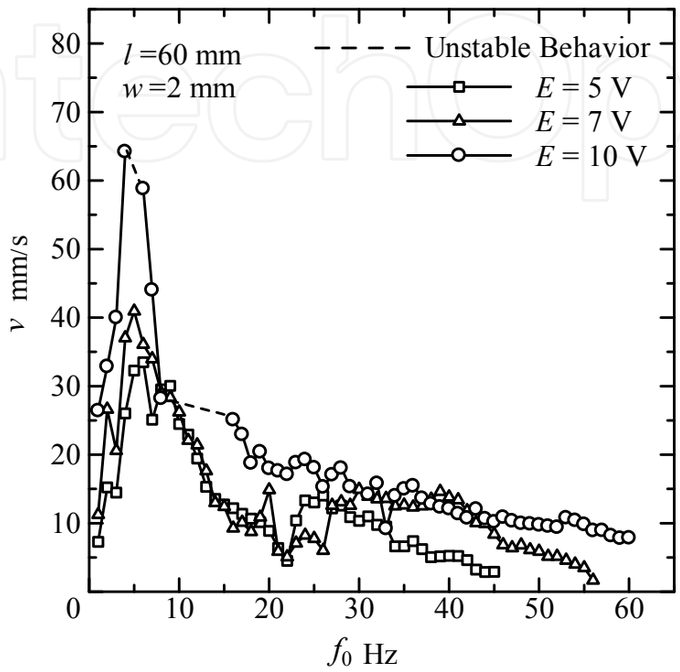

Fig. 18. Frequency characteristics of the micro swimming mechanism

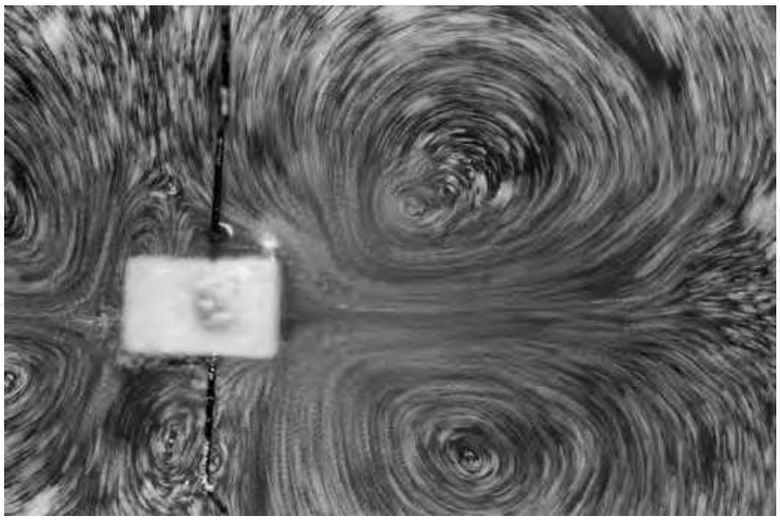

Fig. 19. Flow visualization around the micro swimming mechanism

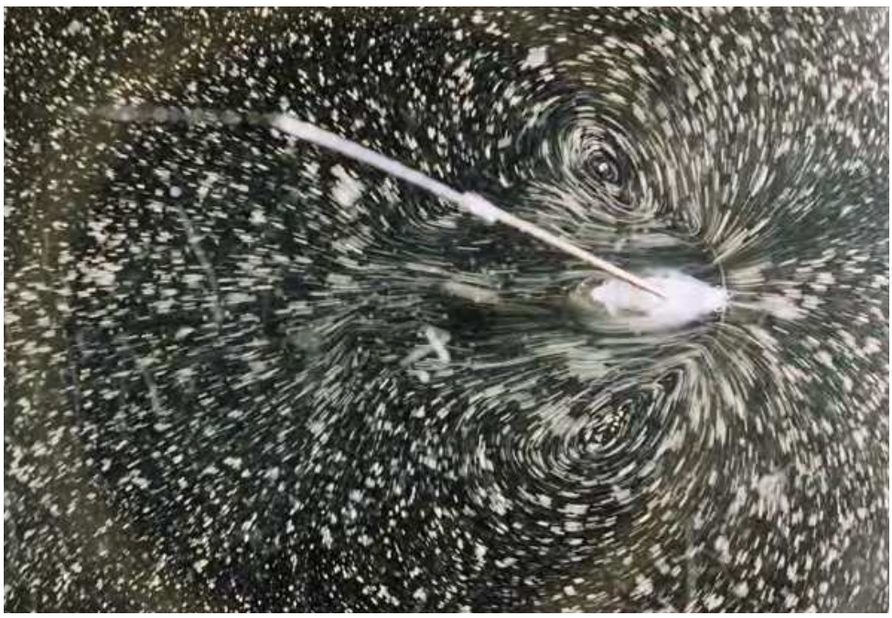

Fig. 20. Flow visualization around a tethered opossum shrimp in dorsal view

generated by beat motion of swimming legs of the opossum shrimp. The opossum shrimp swims forward, by pressing the swimming legs backwards against water. The body length of the opossum shrimp is about 10mm. This photograph was taken with a 35mm camera, shutter speed at 1/15 s.

6. Diving Beetle Robot

The micro swimming robot was developed experimentally based on the analysis of swimming behavior of diving beetle. The swimming robot was propelled by the magnetic torque acting on the small permanent magnet in the external magnetic field. The dimensions of the diving beetle robot are shown in Fig.21. The swimming robot is composed of vinyl chloride body, NdFeB permanent magnet, and polyethyleneterephthalate legs. The external magnetic field was generated by the coil wound round the cylindrical container as shown in Fig.17. Driving mechanism of the diving beetle robot is shown in Fig.22. Arrows in Fig.22 show direction of the physical quantity or direction of the motion. The magnetic torque $\boldsymbol{T}_m$ acting on the permanent magnet with magnetic moment $\boldsymbol{m}$ in the external magnetic field $\boldsymbol{H}$ is given by Eq.(11). The permanent magnet shows the rotational oscillation according to the direction of the alternating magnetic field as shown in Fig.22. In this experiment, the external magnetic field was produced by the coil applied AC voltage. The open and shut motions of the legs occur with the rotational oscillation of the permanent magnet. During such movements the legs press backwards against the water and this pushes the robot forwards. Figure 23 shows frequency characteristics of the diving beetle robot swimming. The swimming velocity of the robot shows the higher value at f_0=4-12 Hz. The maximum value of swimming velocity is v_{max}=29 mm/s. Then swimming number of the diving robot is S_w=0.07. The largest opening angle of the hind leg of real diving beetle is almost $\theta = \pi/2$. However, the angle amplitude of robot leg oscillation is $\xi = 13\pi/180$. Therefore, the

propulsion force produced by leg motion is small. The swimming velocity of the robot was almost 29 mm/s for f_0=4-12 Hz, but it depended on the frequency of the alternating magnetic field.

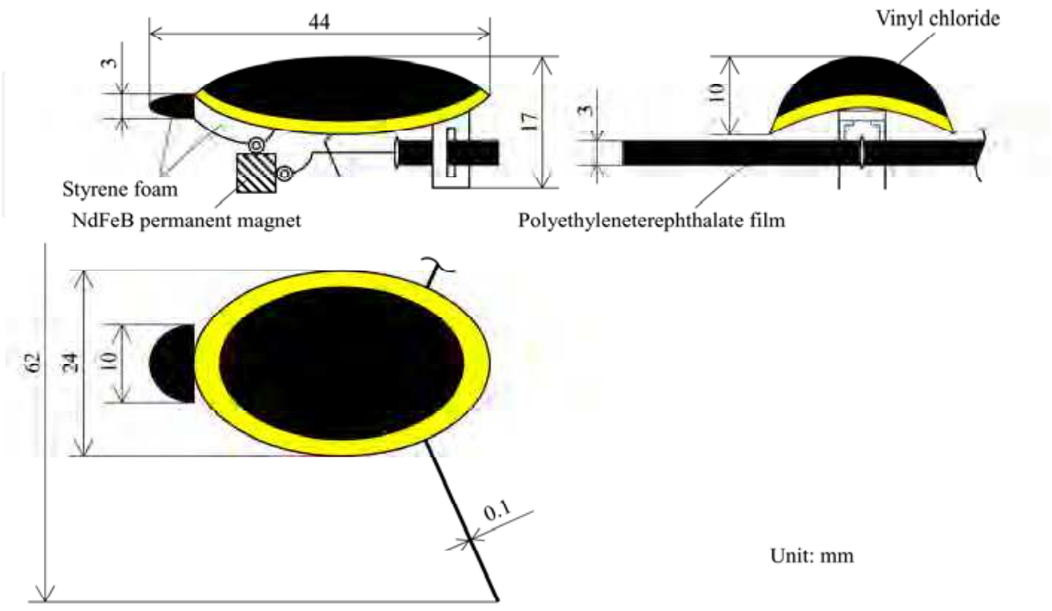

Fig. 21. Schematic diagram and dimensions of micro diving beetle robot

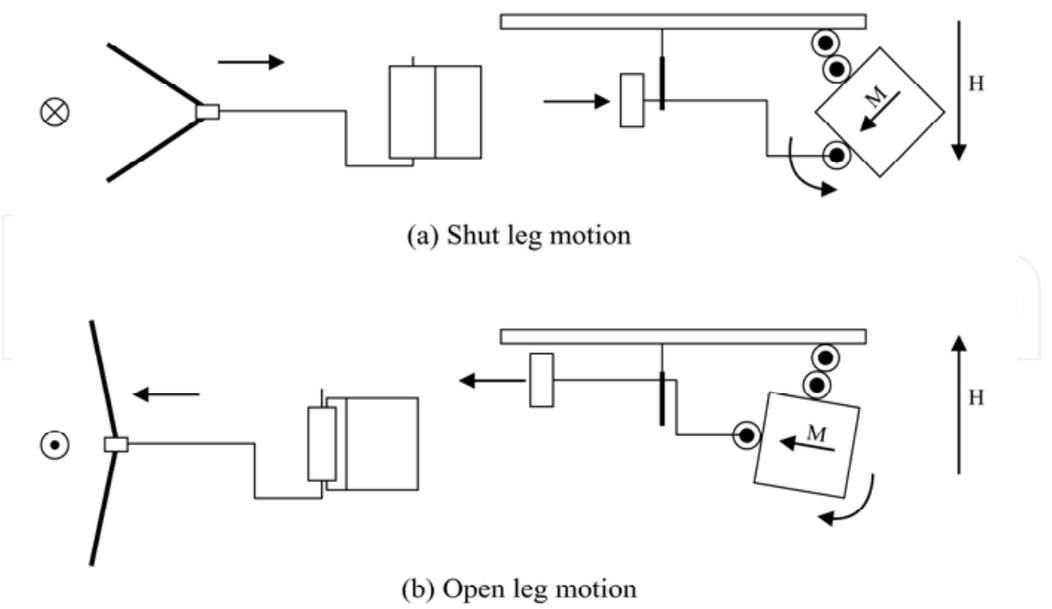

Fig. 22. Driving mechanism of micro diving beetle robot in swimming propursion

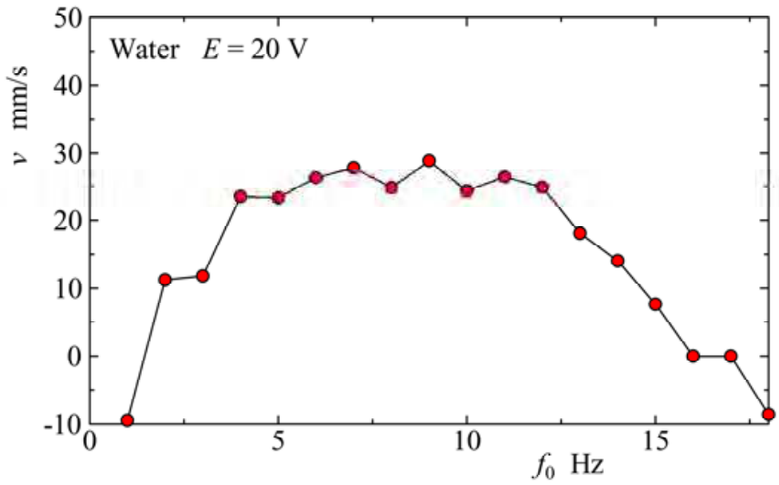

Fig. 23. Frequency characteristics of diving beetle robot in swimming velocity

7. Conclusion

The swimming behavior of small aquatic creatures was analyzed using the high speed video camera system. Based on the swimming analysis of the aquatic creatures, the micro swimming mechanism and micro diving robot propelled by alternating magnetic field were produced. The swimming characteristics of the micro mechanism and micro diving robot were developed. The swimming mechanism and diving robot swam successfully in the water. Frequency characteristics of the swimming mechanism and diving beetle robot were examined. The diving robot showed the higher swimming velocities at f_0=4-12Hz. These experiments show the possibility of achievement of the micro robot driving by the wireless energy supply system. The results obtained are summarized as follows;

(1) In the power stroke of the diving beetle swimming, hind legs are extended and driven backward to generate forward thrust. While in recovery stroke, hind legs are returned slowly to their initial position.
(2) In forward swimming of the dragonfly nymph, only the fore pair and the middle pair of legs are active as a thrust generator. The orbits of fore- and middle-legs show almost the same, and draw the circle partially of the orbit.
(3) The micro swimming mechanism composed of the NdFeB permanent magnet and film fin are driven by the alternating magnetic field. The swimming velocity of the micro mechanism depends on the frequency of alternating magnetic field at the constant voltage.
(4) Flow visualization around the micro mechanism was created by the motion of powder and slow shutter speed photographic technique. The forward and backward surface flows and vortex flows around the micro mechanism were generated by the robot driving.
(5) Visualization photographs of flow field around the tethered opossum shrimp show the generation of tow votices in right and left sides of the body.
(6) The diving robot can dive into the water by sweeping the frequency of magnetic field. The diving robot can swim backward by the change of magnetic field frequency.

8. References

Alexander, R. McN. (1984). The Gaits of Bipedal and Quadrupedal Animals. *The International Journal of Robotics Research*, Vol.3, No.2, pp.49-59

Azuma, A. (1992). *The Biokinetics of Flying and Swimming*, pp.1-265, Springer-Verlag, ISBN 4-431-70106-0, Tokyo

Blake, J. (1972). A model for the micro-structure in ciliated organisms. *Journal of Fluid Mechanics*, Vol.55, pp.1-23

Dickinson, M.H.; Farley, C.T.; Full, R.J.; Koehl, M.A.R.; Kram, R. & Lehman, S. (2000). How animals move: An integrative view. *Science*, Vol.288, No.4, pp.100-106

Dresdner, R.D.; Katz, D.F. & Berger, S.A. (1980). The propulsion by large amplitude waves of untiflagellar micro-organisms of finite length. *Journal of Fluid Mechanics*, Vol.97, pp.591-621

Jiang, H.; Osborn, T.R. & Meneveau, C. (2002a). The flow field around a freely swimming copepod in steady motion. Part I : Theoretical analysis. *Journal of Plankton Research*, Vol.24, No.3, pp.167-189

Jiang, H.; Osborn, T.R. & Meneveau, C. (2002b). The flow field around a freely swimming copepod in steady motion. Part Ⅱ: Numerical simulation. *Journal of Plankton Research*, Vol.24, No.3, pp.191-213

Jiang, H.; Osborn, T.R. & Meneveau, C. (2002c). Chemoreception and the deformation of the active space in freely swimming copepods: a numerical study. *Journal of Plankton Research*, Vol.24, No.5, pp.495-510

Nachtigall, W. (1980a). Mechanics of swimming in water-beetles, In: *Aspects of animal movement*, Elder, H.Y. & Trueman, E.R., pp.107-124, Cambridge University Press, Cambridge

Nachtigall, W. (1980b). Swimming Mechanics and Energetics of Lovomotion of Variously Sized Water Beetles- Dytiscidae, Body Length 2 to 35 mm, In: *Aspects of animal movement,* Elder, H.Y. & Trueman, E.R., pp.269-283, Cambridge University Press, Cambridge

Sudo, S.; Tsuyuki, K. & Honda, T. (2008). Swimming mechanics of dragonfly nymph and the application to robotics. *International Journal of Applied Electromagnetics and Mechanics*, Vol.27, pp.163-175

Sudo, S.; Sekine, K.; Shimizu, M.; Shida, S.; Yano, T. & Tanaka, Y. (2009). Basic Study on Swimming of Small Aquatic Creatures. *Journal of Biomechanical Science and Engineering*, Vol.4, No.1, pp.23-36

Zborowski, P. & Storey, R. (1995). *A Field Guide to Insects in Australia*, pp.111-112, Reed Books Australia, ISBN 0-7301-0414-1, Victoria

Biomimetics Learning from Nature

Edited by Amitava Mukherjee

ISBN 978-953-307-025-4
Hard cover, 534 pages
Publisher InTech
Published online 01, March, 2010
Published in print edition March, 2010

Nature's evolution has led to the introduction of highly efficient biological mechanisms. Imitating these mechanisms offers an enormous potential for the improvement of our day to day life. Ideally, by bio-inspiration we can get a better view of nature's capability while studying its models and adapting it for our benefit. This book takes us into the interesting world of biomimetics and describes various arenas where the technology is applied. The 25 chapters covered in this book disclose recent advances and new ideas in promoting the mechanism and applications of biomimetics.

How to reference

In order to correctly reference this scholarly work, feel free to copy and paste the following:

Seiichi Sudo (2010). Micro Swimming Robots Based on Small Aquatic Creatures, Biomimetics Learning from Nature, Amitava Mukherjee (Ed.), ISBN: 978-953-307-025-4, InTech, Available from: http://www.intechopen.com/books/biomimetics-learning-from-nature/micro-swimming-robots-based-on-small-aquatic-creatures

INTECH
open science | open minds

InTech Europe
University Campus STeP Ri
Slavka Krautzeka 83/A
51000 Rijeka, Croatia
Phone: +385 (51) 770 447
Fax: +385 (51) 686 166
www.intechopen.com

InTech China
Unit 405, Office Block, Hotel Equatorial Shanghai
No.65, Yan An Road (West), Shanghai, 200040, China
中国上海市延安西路65号上海国际贵都大饭店办公楼405单元
Phone: +86-21-62489820
Fax: +86-21-62489821

IntechOpen